



CHORUS

This is the accepted manuscript made available via CHORUS. The article has been published as:

Angularly anisotropic correlation in granular packings

Chengjie Xia, Yixin Cao, Binqun Kou, Jindong Li, Yujie Wang, Xianghui Xiao, and Kamel Fezzaa

Phys. Rev. E **90**, 062201 — Published 1 December 2014

DOI: [10.1103/PhysRevE.90.062201](https://doi.org/10.1103/PhysRevE.90.062201)

Angularly anisotropic correlation in granular packings

Chengjie Xia¹, Yixin Cao¹, Binqun Kou¹, Jindong Li¹ and Yujie Wang^{1*}

¹*Department of Physics and Astronomy, Shanghai Jiao Tong University, 800 Dong Chuan Road, Shanghai 200240, China*

Xianghui Xiao² and Kamel Fezzaa²

²*X-ray Science Division, Argonne National Laboratory, 9700 South Cass Avenue, IL 60439, USA*

We present an X-ray microtomography study of the three-dimensional (3D) structural correlations in monodispersed granular packings. By measuring an orientation-dependent pair correlation function, we found that the local structure shows angularly anisotropic orientation correlation. The correlation is strongest along the major axis of the local Minkowski tensor of the Voronoi cell. It turns out that this anisotropic correlation is consistent with the existence of some locally favored structures. The study suggests the importance of high-order structural correlations in random granular packings.

PACS numbers: 45.70.Cc,87.59.-e

E-mail address: yujiewang@sjtu.edu.cn

I. INTRODUCTION

The nature of random granular packings remains elusive after significant amount of efforts have been devoted to its understanding [1-4]. The difficulty lies in the lacking of a generally accepted theoretical framework. In approaching the packing problem based on statistical mechanics, the theoretical efforts have been carried out

mostly along two lines. A statistical volume ensemble theory was first proposed by Edwards and his coworkers in which the volume has taken the role of energy, and the granular packing samples all mechanical stable states with equal probability [5, 6]. Later, stress has been augmented to simple volume ensembles and both ensembles have been extensively investigated [7-10].

Another line of work has drawn the close analogy between jammed granular packings with thermal glassy systems [11-13]. Especially, a unified jamming phase diagram has been proposed [2, 11]. Recently, it was argued that the jamming transition corresponds to a glassy state at infinite pressure [13], and the jamming transition happens with a finite range of volume fractions [13, 14]. Therefore, the static granular packing problem can be studied using replica method employed in the studies of glass transition [13].

We note that two theoretical approaches are intimately connected as the mechanical stable states in Edwards' ensemble are essentially related to the inherent states of glassy systems [5]. However, both approaches have mostly been carried out at mean-field levels. At finite dimensions, it is generally believed that fluctuations will be significant [15], and the study of the fluctuations is hampered by the fact that the concepts of order and disorder are not well defined [16, 17]. Still, a jammed granular packing show structural features which differ significantly from a "frozen" liquid state: the pair correlation function shows distinct scaling behavior around the contact peak and a split second peak structure [18-20]; the distribution of contact force also shows the development of a peak in the small force regime [21]; a network of strong

and weak force chains develop which show certain correlations [22, 23].

In liquid theory, the correlations can be systematically expanded by including increasing higher orders of correlation functions [24, 25]. In most cases, it is found that simple pair correlation function is sufficient. Recent studies on hard-sphere glass transition which is closely related to random granular packings have focused on the importance of high-order correlation functions including bond orientation order or locally favored structures [26-28]. There also exist approaches of systematical searching for the translational and orientational order [17]. Building upon these approaches and a recent finding that the local environment a particle resides is highly anisotropic [29], we characterize the orientation-dependent pair correlations beyond the standard pair correlation in 3D random granular packings using synchrotron X-ray microtomography [30-32]. We found that the development of the orientation-dependent correlation is in direct correspondence with the development of some locally favored structures, especially structures with approximate five-fold symmetry [33, 34]. Meanwhile, we also characterize the correlations of other parameters like local packing fraction and neighbor number which also involve many-particle information [35, 36].

This paper is organized as follows. In Sec. II we describe the experiment and image processing procedures. In Sec. III we introduce some indices to characterize the anisotropic Voronoi cell around each particle based on one Minkowski tensor [29, 37]. We also quantify the correlations among these structural indices. In Sec. IV we define an orientation-dependent pair correlation function to quantify how local anisotropy is

correlated over several particle diameters. Furthermore, we calculate an orientational entropy associated with this orientation-dependent pair correlation function. In Sec. V we introduce some correlation functions to characterize how local anisotropy indices and Voronoi cells' orientations are spatially correlated. Finally, in Sec. VI, we present some concluding remarks.

II. EXPERIMENT PROCEDURE

In the experiment, the bead packings were prepared by filling a 9 mm ID acrylic cylindrical container to about 1 cm in height using monodispersed glass beads (Duke Scientific, $D = 200 \pm 15 \text{ }\mu\text{m}$). Packings with different packing fractions were obtained by tapping the container using an electromagnetic exciter with different tapping intensity Γ , which is measured by an accelerometer as the ratio between the peak-to-peak acceleration and the gravitational acceleration. The tapping consists of a single cycle of 60-Hz sine wave spaced with 0.5 s intervals to allow the system to relax completely. A total of 1000 taps were applied on each packing with different Γ before the tomography was carried out. The final packing fraction Φ ranges from 0.634 to 0.617 when Γ is increased from 3 to 12 [38].

The X-ray experiment was carried out at the 2BM beamline of the Advanced Photon Source at Argonne National Lab. The “pink” X-ray beam from a bending magnet source with a median energy around 27 keV was utilized for the high-speed tomography image acquisitions. One full tomography scan consists of 1500 projection images. The single exposure time is 30 ms and the full scan lasts about 2 min. The 3D

structures were first reconstructed using the conventional filtered back-projection algorithm. Subsequently, the particles' positions and sizes were acquired by a marker-based watershed image segmentation technique [32]. The reconstructed 3D structure consists of about 17,000 particles in each packing after excluding particles within four particle diameters from the container boundary. In this following, for brevity, all physical lengths are expressed in units of average particle diameter.

III. STRUCTURAL ANISOTROPY

The local structure of the packing is ordinarily characterized by Voronoi tessellation. Local packing fraction $\Phi_{loc} = w_0 / w_{cell}$ (w_0 and w_{cell} are volumes of the particle and its Voronoi cell) and Voronoi neighbor number N (numbers of particles sharing a common Voronoi cell surface with the central particle) are calculated to quantify the local environment of a granular particle. In addition to above scalar parameters, the shape of the Voronoi cell was analyzed using a Minkowski tensor $W_1^{0,2}$ defined as the surface integral of the tensor-valued self-product of the bounding surface normal \mathbf{n} [29, 37]:

$$W_1^{0,2} = \int \mathbf{n} \otimes \mathbf{n} dA. \quad (1)$$

The tensor representation allows an explicit depiction of the cell's anisotropy. The eigenvalues of $W_1^{0,2}$ are listed as $(\varepsilon_1, \varepsilon_2, \varepsilon_3)$ with $\varepsilon_1 > \varepsilon_2 > \varepsilon_3$ without loss of generality. To characterize the cell's shape anisotropy, the anisotropy index $\beta = \varepsilon_3 / \varepsilon_1$ is introduced [29]. The value of β ranges from one (isotropic shape) to zero (a line or a plane). Additionally, another anisotropy index $\gamma = (\varepsilon_2 - \varepsilon_3) / (\varepsilon_1 - \varepsilon_3)$

is introduced to characterize the degeneracy of the three eigenvalues. The value of γ also ranges from zero (perfect oblate cell) to one (perfect prolate cell). The probability distribution functions (PDF) of β and γ for packing with $\Phi = 0.634$ are shown in Fig. 1 (a) and (b). The PDFs suggest that the Voronoi cells are mostly anisotropic and consist of both prolate and oblate shapes. Averaged β and γ for different packing fractions Φ were calculated and shown in the insets of Fig. 1 (a) and (b). Similar to previous findings [29], $\langle\beta\rangle$ increases for higher Φ , while $\langle\gamma\rangle$ is almost constant for different Φ .

In the following, we demonstrate that β and γ are structural indices that carry local structural information of the amorphous packing beyond other standard local structural indices. In addition to local packing fraction Φ_{loc} and Voronoi neighbor number N , we calculate bond orientational order parameters Q_4 , Q_6 , and three other order metrics Δ_{fcc} , Δ_{hcp} , and Δ_{icos} [28, 39]. The last three order metrics are calculated from a rank-four Minkowski tensor of a Voronoi cell, in which Δ_{fcc} (Δ_{hcp} , or Δ_{icos}) is the root-mean-square of the difference between the six eigenvalues of this rank-four tensor and those of perfect face-centered-cubic crystalline (hexagonal-close-packing or quasi-crystalline icosahedral) cluster [39]. These order metrics are sensitive in identifying local crystalline clusters [39]. The linear correlation coefficients among above structural indices for packing with $\Phi = 0.634$ are shown in Table I. We note that the anisotropy index β is correlated with Φ_{loc} and N , but is almost uncorrelated with those indices quantifying local crystalline orders. γ seems to be uncorrelated with all other local indices. Specifically, we

show the scattered plots and conditional averages of Φ_{loc} , N , Q_4 and Q_6 for different β in Fig. 2. The averages of all indices show monotonic dependencies upon β , but the correlations are rather weak. Similar relationships apply for all other structural indices.

IV. ORIENTATIONAL CORRELATION

A. Orientation-dependent pair correlation function

In addition to β and γ , we also calculate the local orientation of each Voronoi cell from $W_1^{0,2}$. We calculate the eigenvectors corresponding to the eigenvalues of $W_1^{0,2}$: the major axis e_M and minor axis e_m corresponds to ε_1 and ε_3 respectively. The global distributions of e_M and e_m are uniform in all directions, suggesting that the packing is isotropic globally. However, it turns out that the anisotropy of Voronoi cell is not localized within the first shell, but is spatially correlated and affects the structures in a range of about three to four particle diameters around the central particle.

In the following, we introduce a set of orientation-dependent correlation functions to quantify such anisotropic spatial correlations. First we augment the standard pair correlation function $g(r)$ into an orientation-dependent pair correlation function $g(r, \theta, \varphi)$. A local Cartesian coordinate system for each particle was set up based on e_M and e_m : e_M is the z -axis, e_m is the x -axis, and $e_M \times e_m$ is the y -axis as shown in Fig. 3 (a). A local spherical coordinate system is further defined based upon the Cartesian coordinate system. In the spherical coordinate system, the relative

positions and orientations of two particles' Voronoi cells can be expressed using six independent variables: $(r_{ij}, \theta_{ij}, \varphi_{ij})$ represents the relative position of particle j in the coordinate system of particle i , and another three variables represents the relative orientations of the two Voronoi cells.

For simplicity, we first neglect the relative orientation of two Voronoi cells and calculate an orientation-dependent pair correlation function $g(r, \theta, \varphi)$ defined as:

$$g(r, \theta, \varphi) = \frac{1}{4\pi r^2 \rho \Delta r \Delta \Omega} \langle \delta(r - r_{ij}) \delta(\theta - \theta_{ij}) \delta(\varphi - \varphi_{ij}) \rangle, \quad (2)$$

where the average is taken for all pairs of particles. ρ is the number density of the packing. Δr is the increment of r and $\Delta \Omega$ is the size of solid angle centering at (θ, φ) . Due to the symmetry between $(\theta, \pi - \theta)$, $(\varphi, \pi - \varphi)$ and $(\varphi, -\varphi)$, we map all data to $\theta, \varphi \in [0, \pi/2]$ and average data from equivalent ranges. Since $g(r, \theta, \varphi)$ is a function with three variables, we plot it using a set of 2D colormaps as shown in Fig. 3 where different colors are used to indicate the intensity of correlations. As comparison, the ordinary pair correlation function $g(r)$ is also plotted in Fig. 3 (b). We plot $g(r, \theta, \varphi)$ on $\varphi = 0$ plane, $\varphi = \pi/2$ plane, and $\theta = \pi/2$ plane. These colormaps clearly demonstrate that pair correlation function is strongest along the major axis and weakest along the minor axis and the correlation extends to several particle diameters. Furthermore, we show $g(r, \theta, \varphi)$ at given r ($g(r = \sqrt{3}, \theta, \varphi)$ and $g(r = 2, \theta, \varphi)$). $r = \sqrt{3}$ and $r = 2$ are chosen as the positions of two sub-peaks in the split second peak of $g(r)$ (see Fig. 3 (b)). It was evident that $r = \sqrt{3}$ peak is highest along e_M while $r = 2$ peak is relatively uniform angularly.

B. Anisotropic local configurations

In this section, we try to establish the connection between the local anisotropy and its spatial correlation with some locally favored structures. As pointed out before [33], pair correlation function $g(r)$ can be decomposed into the contributions of various local configurations, defined as $ijkl$ pairs. $ijkl$ pairs were identified by a classification of the geometry of the common neighbors of pairs of particles. Neighboring particles (or bonded particles) were defined with a cut-off distance $r_c = 1.34$ which corresponds to the first minimum of $g(r)$. Index j corresponds to the number of common neighbors to the pair of particles. Index k is the number of bonds among the j common neighbors. Index l is the length of the longest continuous chain formed by the k bonds [33]. Motivated by this approach, we calculate the orientations of these $ijkl$ pairs and compare them with e_M and e_m .

For each pair, we calculate the angle θ_M (θ_m) between the pair's relative direction and the corresponding individual e_M (e_m) of the two particles. $f_{ijkl}(\theta_M)$ is the PDF of θ_M for some specific $ijkl$ types, and we plot $\frac{f_{ijkl}(\theta_M)}{\sin \theta_M}$ versus θ_M in polar coordinates as shown in Fig. 4, where $\sin \theta_M$ is a normalization factor. Similar diagrams were also shown for θ_m . We present the results of 555, 544 and 433 pairs corresponding to the first peak of $g(r)$ [33]. 555 pair is a part of icosahedral arrangement of 13 particles while 544 and 433 pairs correspond to a part of distorted icosahedral order. As illustrated in Fig. 4 (a) and (b), 555 pair shows the best alignment with e_M compared with other pairs. We also show the results of 333, 211 and 100 pairs which correspond to the second peak of $g(r)$ (Fig. 4 (c) and (d)). 333 pair shows the best alignment with e_M while the

orientations of other two types of pairs show comparatively uniform distributions. 333 pair is a bi-pyramid cluster of two tetrahedral configurations, which is also a local dense structure and a part of icosahedral arrangement. We notice that the above 555 and 333 pairs correspond to $7A$ and $5A$ clusters in the topological cluster classification method [27]. Above calculation suggests that locally dense structures with five-fold symmetry serve as the major contribution to local anisotropy and its spatial correlations.

We further verified that the choice of the cut-off distance r_c in the range [1.3,1.5] has only minor effects on above results, *i.e.*, if neighboring particles were defined based on Voronoi cell connection or a recent parameter-free method [40], the corresponding numbers of different particle pair types would change, but the PDFs of θ_M (θ_m) only show minor differences.

C. Orientational entropy

The anisotropic local structures of random granular packings suggest the existence of some orientational degrees of freedom. These degrees of freedom and their correlations should contribute to a non-trivial part of the configurational entropy of the packing. Motivated by the calculations of the configurational entropy for liquids with anisotropic molecules [41], we define an orientational distribution function $g_o(\theta, \varphi|r)$ according to the decomposition of $g(r, \theta, \varphi)$ into translational and orientational part:

$$g(r, \theta, \varphi) = g_t(r) g_o(\theta, \varphi|r), \quad (3)$$

and

$$g_t(r) = \frac{1}{4\pi} \int g(r, \theta, \varphi) \sin \theta d\theta d\varphi \quad (4)$$

is the ordinary radial distribution function $g(r)$.

Afterwards, the two-particle term in the entropy expression can also be decomposed into translational and orientational part: $s = s_t + s_o$ with:

$$s_t = -\frac{4\pi}{2} \rho \int [g_t(r) \log g_t(r) - g_t(r) + 1] r^2 dr, \quad (5)$$

and

$$s_o = 4\pi\rho \int g_t(r) S_o(r) r^2 dr, \quad (6)$$

where

$$S_o(r) = -\frac{1}{8\pi} \int g_o(\theta, \varphi|r) \log g_o(\theta, \varphi|r) \sin \theta d\theta d\varphi. \quad (7)$$

In above calculations, the Boltzmann constant is set to unity. The integration range in both Eq. (5) and (6) is $[0, +\infty)$. In reality, a range $[0, 8]$ is sufficient. The translational and orientational entropy s_t and s_o were calculated for packing with different packing fractions as shown in Fig. 5 (a) and (b). Decreasing of both entropies with increasing packing fraction towards the random close packing limit $\Phi \approx 0.64$ was observed [18], which suggests that jamming transition is accompanied with increasing ordering in both translational and orientational degrees of freedom. The absolute value of s_o is about one-order of magnitude smaller than that of s_t . It is worth noting that the anisotropy of a local cell is due to the multiple particle correlations and therefore $g(r, \theta, \varphi)$ by nature corresponds to a multi-to-one-particle correlation. Therefore, s_o calculated from $g(r, \theta, \varphi)$ corresponds to some high-order expansion of the configurational entropy omitted in the ordinary pair

correlation function $g(r)$.

Furthermore, we calculate the contributions to s_t and s_o from nearest neighbors by defining $s_{t,nn}$ and $s_{o,nn}$ which has an integration range from $[0, 1.34]$ in Eqs. (5) and (6). We plot the relative contribution to the total entropy from nearest neighbor particles: $s_{t,nn}/s_t$ and $s_{o,nn}/s_o$ as a function of Φ in the insets of Fig. 5 (a) and (b). Particle arrangements of nearest neighbors contribute about 45% to s_o which suggests that the orientational correlation mainly comes from the anisotropy beyond first shell, while translational correlation beyond first shell is comparatively smaller. Both $s_{t,nn}/s_t$ and $s_{o,nn}/s_o$ decrease with increasing Φ suggesting that correlations get more long-ranged towards random close packing.

V. CORRELATION OF VORONOI CELLS

A. Correlation of cell orientation

For even higher order orientational correlations, we focus on the spatial correlation between the orientations of eigenvectors between pairs of particles. As noted above, the correlation of particle positions is relatively strong along the major axis of $W_1^{0,2}$, we therefore presume that the meso-scale anisotropy in sphere packings mainly exists along \mathbf{e}_M . We then calculate the orientational correlation between \mathbf{e}_M for pairs of particles, and neglect the correlations of other two axes.

This orientational correlation function is defined as:

$$o(r, \theta, \varphi) = \left\langle \frac{3(\mathbf{e}_{M,i} \cdot \mathbf{e}_{m,i})^2 - 1}{2} \delta(r - r_{ij}) \delta(\theta - \theta_{ij}) \delta(\varphi - \varphi_{ij}) \right\rangle \quad (8)$$

where the average is taken for all pairs of particles and $\mathbf{e}_{M,i}$ is the major axis of

particle i . The $\frac{3(\overrightarrow{e_{M,i}} \cdot \overrightarrow{e_{M,j}})^2 - 1}{2}$ term is in analogy with nematic order parameter in liquid crystals. $o(r, \theta, \varphi)$ is illustrated in Fig. 6. Similar to $g(r, \theta, \varphi)$, the orientational correlation between major axes is also stronger along \mathbf{e}_M for each particle, while the variation of $o(r, \theta, \varphi)$ for different φ seems comparatively weak. The oscillatory behavior of $o(r, \theta, \varphi)$ along \mathbf{e}_M suggests that the orientations of \mathbf{e}_M for neighboring particles exhibit an alternating tendency between being parallel and orthogonal with \mathbf{e}_M of the central particle and extend to about three particle diameters. We also calculate the correlation of the orientations of minor axes of pairs of particles and found that the correlation extends to only about 1.5 particle diameters.

The estimation of configurational entropy associated with this non-uniform distribution of the orientation between \mathbf{e}_M or even \mathbf{e}_m is beyond the scope of this work. However, as s_o is contributed by multi-to-one-particle correlation and above $o(r, \theta, \varphi)$ correlation is contributed by multi-to-multi-particle correlation, we presume that its contribution to total configurational entropy should be much smaller than s_o .

B. Correlation of cell anisotropy

Finally, to fully quantify the meso-scale anisotropic structures of sphere packings, we further calculate the spatial correlations of anisotropy indices β and γ . For simplicity, we neglect the variation of spatial correlation in (θ, φ) degrees of freedom and the correlation function becomes isotropic:

$$c_a(r) = \left\langle \frac{(a_i - \langle a \rangle)(a_j - \langle a \rangle)}{\text{var}(a)} \delta(r - r_{ij}) \right\rangle \quad (9)$$

where a represents a specific structure quantity ($a = \beta, \gamma, \Phi, N$, etc.) and the average is taken for all pairs of particles. $\langle a \rangle$ and $\text{var}(a)$ are the average value and variation of a respectively. As shown in Fig. 7, β shows positive correlation within two particle diameters while the γ correlation is basically zero. This suggests that anisotropic cells tend to locate near anisotropic ones while the degeneracy of eigenvalues seems uncorrelated. Together with the analysis of the correlation between γ and other structural quantities, it seems that whether the shape of the Voronoi cell is close to an oblate ellipsoid or a prolate one is unimportant. As comparison, we calculate $c_\Phi(r)$ and $c_N(r)$ as well (Fig. 7). It was shown that all these scalar structural parameters has a spatial correlation of about two particle diameters, which is close to the correlation length of $o(r, \theta, \varphi)$, while the correlation length of $g(r, \theta, \varphi)$ along e_M is slightly longer.

V. DISCUSSION AND CONCLUSIONS

In summary, the non-uniform angular distribution of neighboring particles results in an anisotropic local structure of sphere packings. This anisotropy is well characterized through some anisotropy indices. In the current study, by using an orientation-dependent pair correlation function, we find that this anisotropy structure extends beyond first shell, and shows an anisotropic correlation extending to several particle diameters with the maximum correlation along the major axis of local Minkowski tensor.

The current study bridges the approaches of studying the packing structure using topological classification [27] and systematic expansion beyond pair correlation functions [24]. By decomposing the standard pair correlation function into translational and orientational parts, we can investigate their individual contributions to the correlations in the system, and clearly established the connection with the topological structural analysis.

However, there are two points need caution. The first is that the preferred correlation along the major axis only suggests a strong correlation along a fixed direction while in reality the true correlation in amorphous systems might not follow a straight line [42]. Therefore, the actual correlation could be even longer. Secondly, in defining the neighbors, the method of a cut-off distance has been adopted which follows the custom in systems with short-range attractive interactions in which the local cluster structures correspond to the local minima of the energy landscape [27]. For hard sphere systems, the interactions are purely repulsive. Therefore, how to establish the connections between local anisotropy, particular local structures, and their free energy implications remain elusive.

The current study also brings interesting connections with packings of anisotropic particles, which have orientational degrees of freedom intrinsically [43, 44]. Additionally, the local anisotropic correlations could also be related to force chains [22, 23]. How to relate structure with force information will be of great interest in the future.

ACKNOWLEDGEMENTS

We appreciate helpful discussion with Yuliang Jin. This work and the use of the APS are supported by the U.S. Department of Energy, Office of Science, Office of Basic Energy Sciences, under contract No. DE-AC02-06CH11357. Some of the preliminary experiments have been carried out at BL13W1 beamline of the Shanghai Synchrotron Radiation Facility (SSRF). The work is supported by the Chinese National Science Foundation Nos. 11175121, National Basic Research Program of China (973 Program; 2010CB834301).

- [1] J. Bernal and J. Mason, *Nature* **188**, 910 (1960).
- [2] A. J. Liu and S. R. Nagel, *Annu. Rev. Cond. Matt. Phys.* **1**, 347 (2010).
- [3] S. Torquato and F. Stillinger, *Rev. Mod. Phys.* **82**, 3197 (2010).
- [4] M. P. Ciamarra, P. Richard, M. Schröter, and B. P. Tighe, *Soft Matter* **8**, 9731 (2012).
- [5] S. F. Edwards and R. Oakeshott, *Physica A* **157**, 1080 (1989).
- [6] A. Mehta and S. Edwards, *Physica A* **157**, 1091 (1989).
- [7] S. Edwards and D. Grinev, *Phys. Rev. Lett.* **82**, 5397 (1999).
- [8] R. C. Ball and R. Blumenfeld, *Phys. Rev. Lett.* **88**, 115505 (2002).
- [9] S. Henkes and B. Chakraborty, *Phys. Rev. Lett.* **95**, 198002 (2005).
- [10] H. A. Makse and J. Kurchan, *Nature* **415**, 614 (2002).
- [11] A. J. Liu and S. R. Nagel, *Nature* **396**, 21 (1998).
- [12] R. D. Kamien and A. J. Liu, *Phys. Rev. Lett.* **99**, 155501 (2007).
- [13] G. Parisi and F. Zamponi, *Rev. Mod. Phys.* **82**, 789 (2010).
- [14] P. Chaudhuri, L. Berthier, and S. Sastry, *Phys. Rev. Lett.* **104**, 165701 (2010).
- [15] Y. Jin, J. G. Puckett, and H. A. Makse, *Phys. Rev. E* **89**, 052207 (2014).
- [16] S. Torquato, T. M. Truskett, and P. G. Debenedetti, *Phys. Rev. Lett.* **84**, 2064 (2000).
- [17] T. M. Truskett, S. Torquato, and P. G. Debenedetti, *Phys. Rev. E* **62**, 993 (2000).
- [18] C. S. O'Hern, L. E. Silbert, A. J. Liu, and S. R. Nagel, *Phys. Rev. E* **68**, 011306 (2003).
- [19] A. Donev, S. Torquato, and F. H. Stillinger, *Phys. Rev. E* **71**, 011105 (2005).
- [20] L. E. Silbert, A. J. Liu, and S. R. Nagel, *Phys. Rev. E* **73**, 041304 (2006).
- [21] C. S. O'Hern, S. A. Langer, A. J. Liu, and S. R. Nagel, *Phys. Rev. Lett.* **86**, 111 (2001).
- [22] T. S. Majmudar and R. P. Behringer, *Nature* **435**, 1079 (2005).
- [23] F. Radjai, D. Wolf, M. Jean, and J. Moreau, *Phys. Rev. Lett.* **80**, 61 (1998).
- [24] J. P. Hansen and I. R. McDonald, *Theory of simple liquids* (1990).
- [25] D. C. Wallace, *J. Chem. Phys.* **87**, 2282 (1987).
- [26] H. Tanaka, T. Kawasaki, H. Shintani, and K. Watanabe, *Nature Mater.* **9**, 324 (2010).
- [27] C. P. Royall, S. R. Williams, T. Ohtsuka, and H. Tanaka, *Nature Mater.* **7**, 556 (2008).
- [28] P. J. Steinhardt, D. R. Nelson, and M. Ronchetti, *Phys. Rev. B* **28**, 784 (1983).
- [29] G. E. Schröder-Turk, W. Mickel, M. Schröter, G. W. Delaney, M. Saadatfar, T. J. Senden, K. Mecke, and T. Aste, *Europhys. Lett.* **90**, 34001 (2010).
- [30] P. Richard, P. Philippe, F. Barbe, S. Bourlès, X. Thibault, and D. Bideau, *Phys. Rev. E* **68** (2003).
- [31] T. Aste, M. Saadatfar, and T. Senden, *Phys. Rev. E* **71** (2005).
- [32] Y. X. Cao, B. Chakraborty, G. C. Barker, A. Mehta, and Y. J. Wang, *Europhys. Lett.* **102**, 24004 (2013).
- [33] A. S. Clarke and H. Jónsson, *Phys. Rev. E* **47**, 3975 (1993).
- [34] A. Anikeenko and N. Medvedev, *Phys. Rev. Lett.* **98**, 235504 (2007).
- [35] T. Aste and T. Di Matteo, *Eur. Phys. J. E* **22**, 235 (2007).

- [36] S. C. Zhao, S. Sidle, H. L. Swinney, and M. Schröter, *Europhys. Lett.* **97**, 34004 (2012).
- [37] G. E. Schröder-Turk, W. Mickel, S. C. Kapfer, M. A. Klatt, F. M. Schaller, M. J. F. Hoffmann, N. Kleppmann, P. Armstrong, A. Inayat, D. Hug, M. Reichelsdorfer, W. Peukert, W. Schwieger, and K. Mecke, *Adv. Mater.* **23**, 2535 (2011).
- [38] E. R. Nowak, J. B. Knight, M. L. Povinelli, H. M. Jeager, and S. R. Nagel, *Powder Technol.* **94**, 79(1997).
- [39] S. C. Kapfer, W. Mickel, K. Mecke, and G. E. Schröder-Turk, *Phys. Rev. E* **85** (2012).
- [40] Z. A. Tian, R. S. Liu, K. J. Dong and A. B. Yu, *Europhys. Lett.* **96**, 36001, (2011).
- [41] T. Lazaridis and M. Karplus, *J. Chem. Phys.* **105**, 4294 (1996).
- [42] T. Tomida and T. Egami, *Phys. Rev. B* **52**, 3290 (1995).
- [43] A. Donev, I. Cisse, D. Sachs, E. A. Variano, F. H. Stillinger, R. Connelly, S. Torquato, and P. M. Chaikin, *Science* **303**, 990 (2004).
- [44] C. Xia, K. Zhu, Y. Cao, H. Sun, B. Kou, and Y. Wang, *Soft Matter* **10**, 990 (2014).

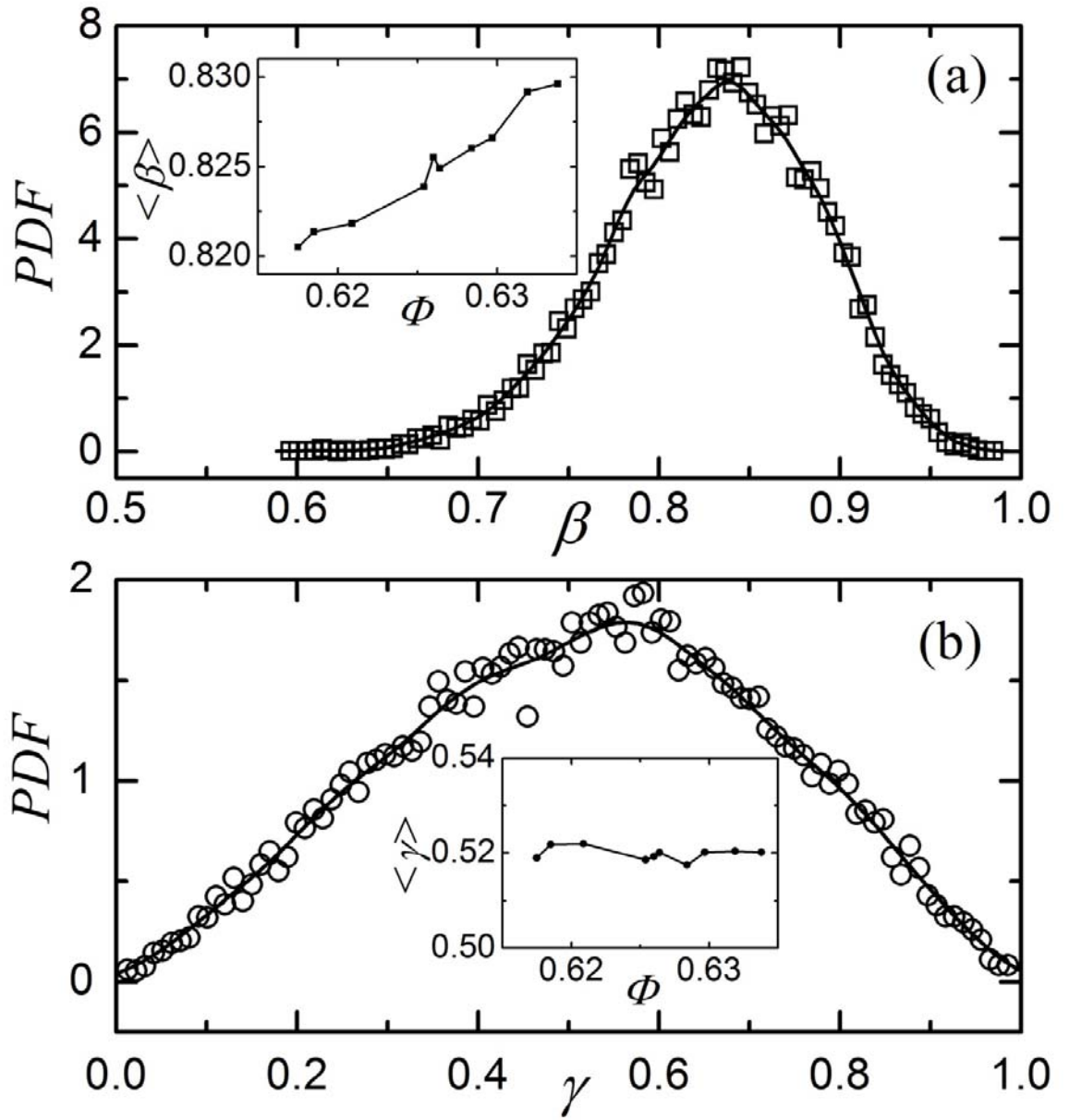


FIG. 1. PDFs of β (a) and γ (b) for packing with $\Phi = 0.634$. The insets show the averaged value $\langle \beta \rangle$ v.s. Φ (a) and $\langle \gamma \rangle$ v.s. Φ (b).

	β	γ	Φ_{loc}	N	Q_4	Q_6	Δ_{fcc}	Δ_{hcp}	Δ_{icos}
β	1	-0.044	0.253	-0.251	-0.122	0.118	-0.049	-0.049	-0.034
γ	-	1	0.016	-0.019	0.014	0.080	-0.013	-0.011	-0.008
Φ_{loc}	-	-	1	-0.187	-0.265	0.063	-0.227	-0.290	-0.290
N	-	-	-	1	-0.093	-0.580	0.146	0.172	0.173
Q_4	-	-	-	-	1	0.183	0.328	0.510	0.511
Q_6	-	-	-	-	-	1	-0.137	-0.175	-0.181
Δ_{fcc}	-	-	-	-	-	-	1	0.706	0.657
Δ_{hcp}	-	-	-	-	-	-	-	1	0.990
Δ_{icos}	-	-	-	-	-	-	-	-	1

TABLE I. Correlation matrix for various structural indices. This matrix is symmetric thus the data in the lower half are not shown.

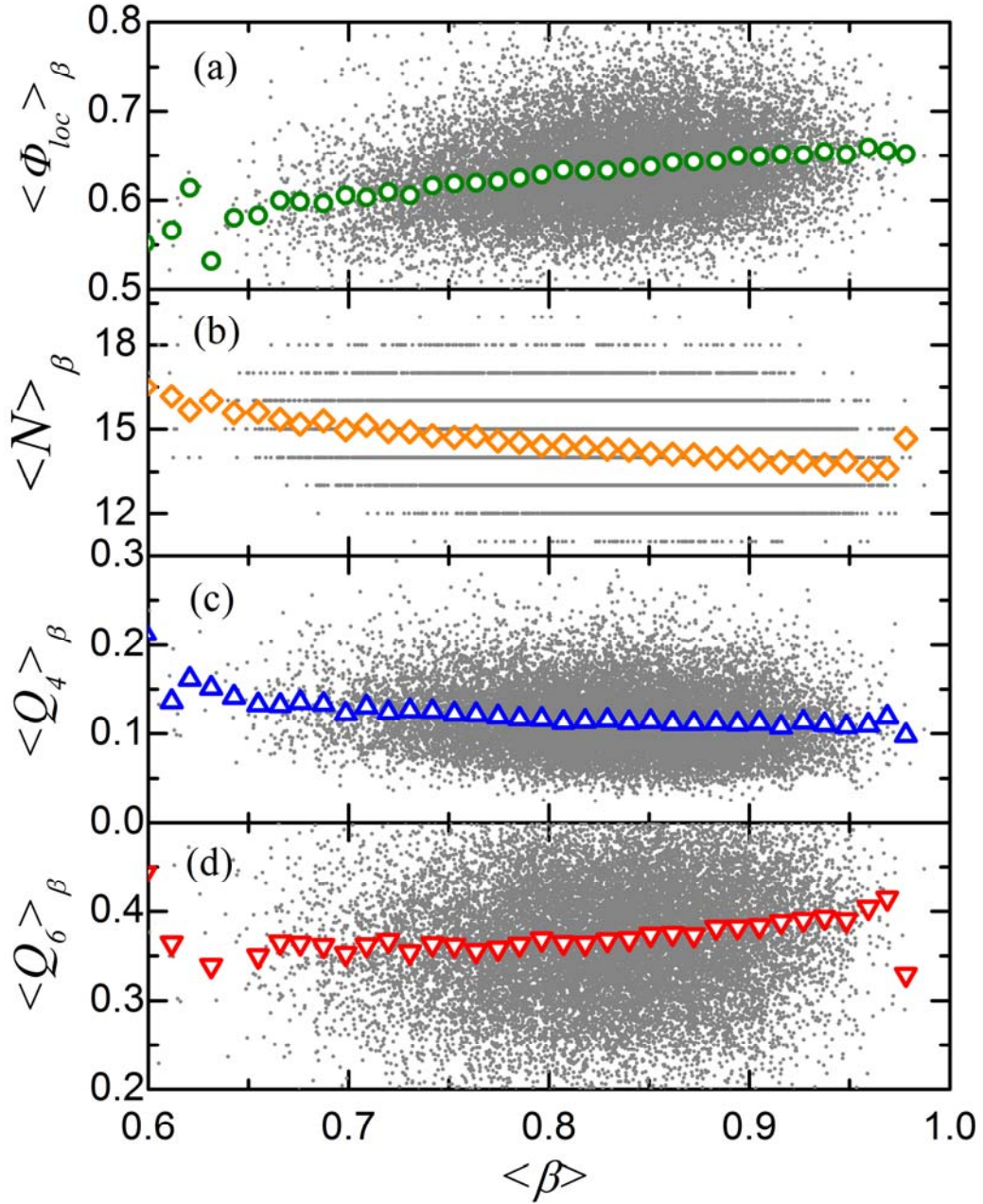


FIG. 2. Conditional average of (a) Φ_{loc} , (b) N , (c) Q_4 and (d) Q_6 for given values of β . The gray scattered points are the unaveraged data points.

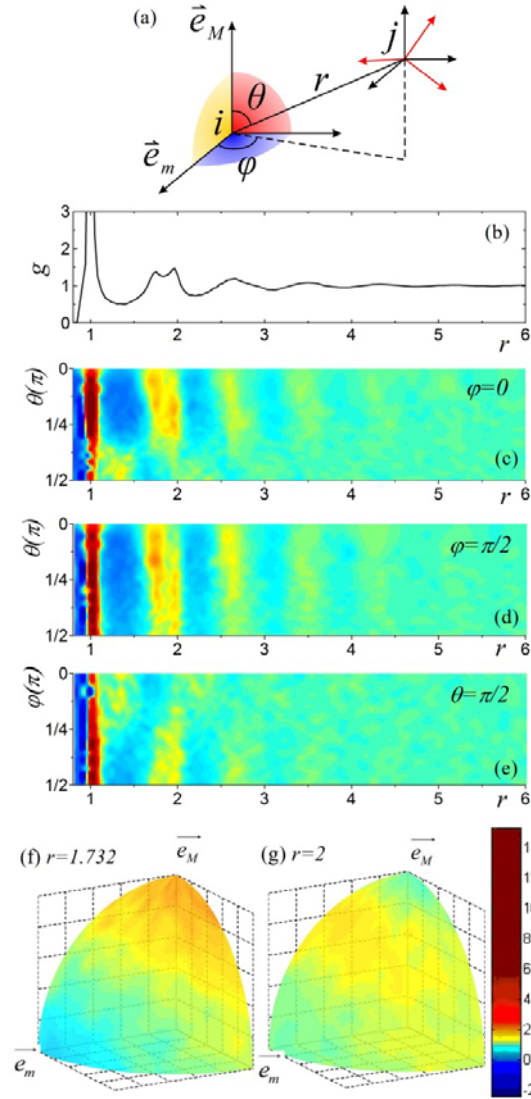


FIG. 3. (Color online) (a) A schematic for the local coordinate system of particle i , and the relative position and orientation of particle j . The red coordinate system marks the orientations of the axes of particle j . (b) Ordinary pair correlation function $g(r)$. (c,d,e,f,g) Orientation-dependent pair correlation function $g(r, \theta, \varphi)$ shown on (c) $\varphi = 0$ plane (yellow plane in panel (a)), (d) $\varphi = \pi/2$ plane (red plane in panel (a)), (e) $\theta = \pi/2$ plane (blue plane in panel (a)), (f) $r = \sqrt{3}$ spherical surface and (g) $r = 2$ spherical surface.

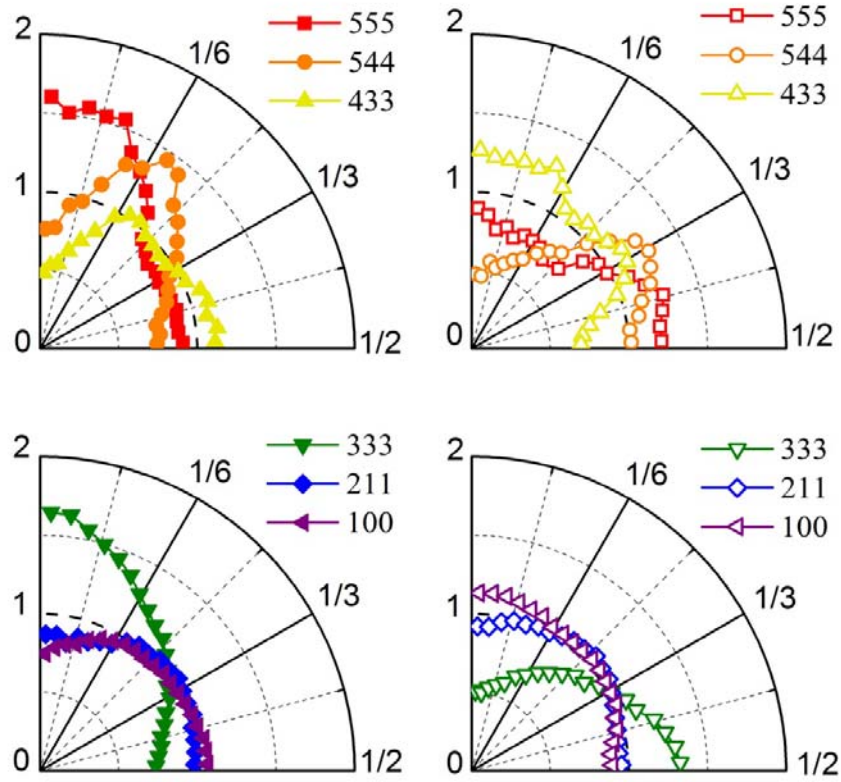


FIG. 4. (Color online) Angles between various jkl pairs and \overline{e}_M (solid symbols) or \overline{e}_m (open symbols). Data for following types of pairs are shown: 555 (square), 544 (circle), 433 (up triangle), 333 (down triangle), 211 (diamond), and 100 (left triangle) pairs.

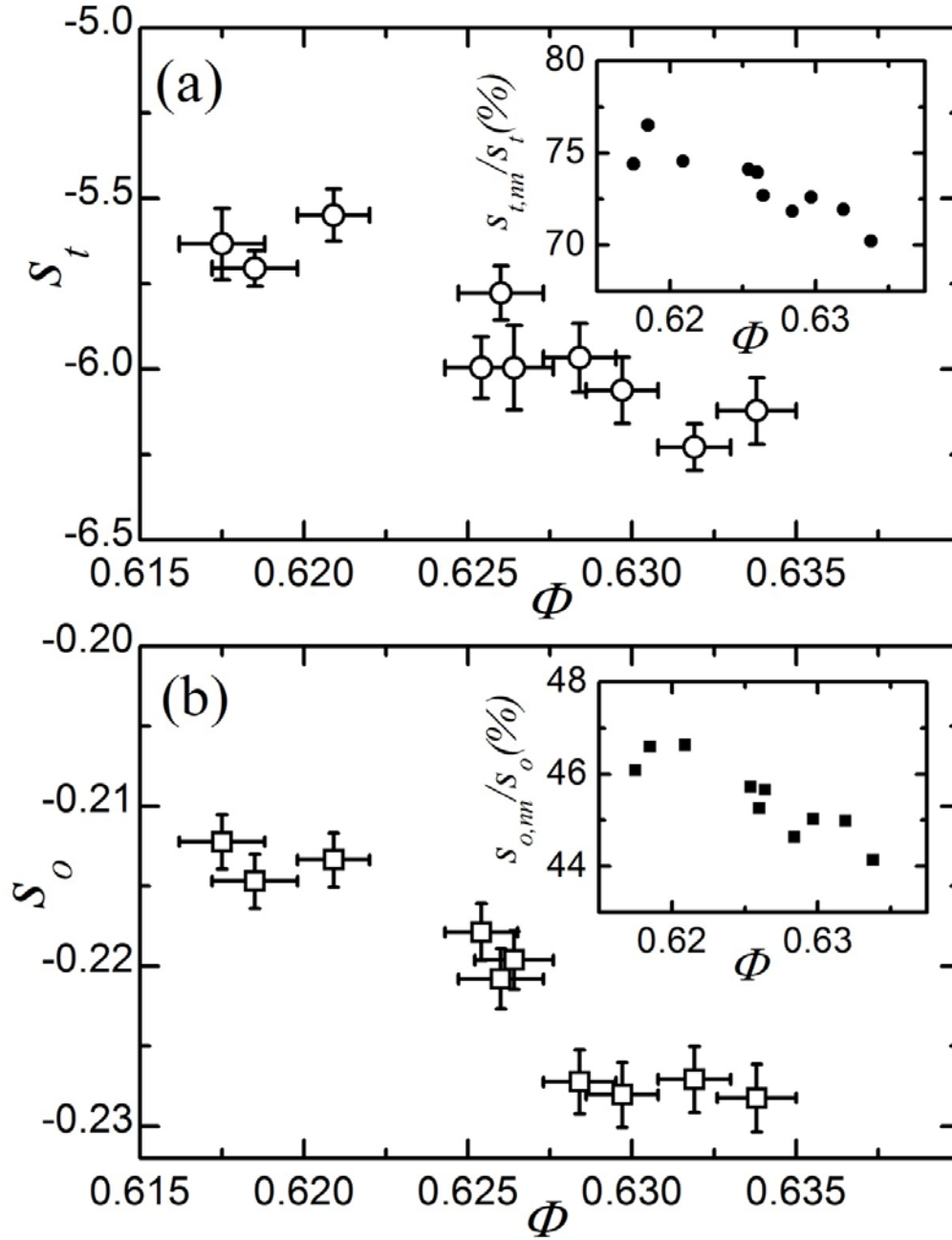


FIG. 5. Translational (a) and orientational (b) entropy for packings with different Φ .

Insets: Relative contributions to translational (a) and orientational (b) entropy from

nearest neighbors for packings with different Φ .

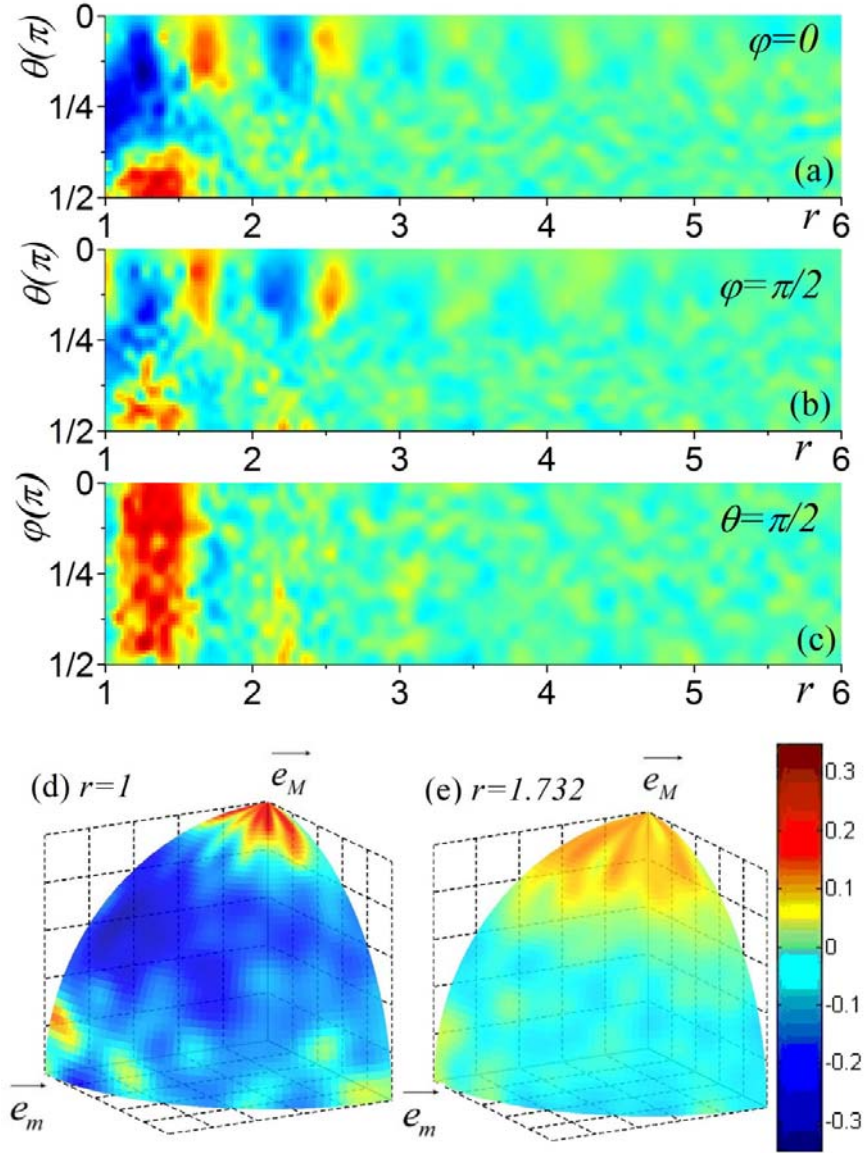


FIG. 6. (Color online) Orientation-dependent correlation function $o(r, \theta, \varphi)$ shown on (a) $\varphi = 0$ plane, (b) $\varphi = \pi/2$ plane, (c) $\theta = \pi/2$ plane, (d) $r = 1$ spherical surface and (e) $r = \sqrt{3}$ spherical surface.

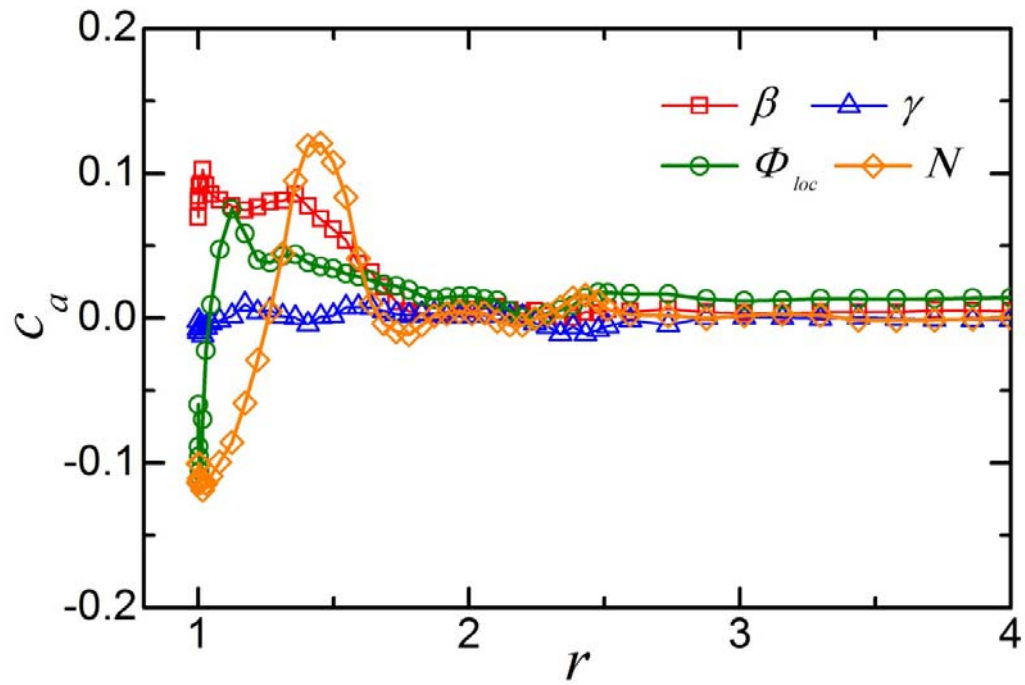


FIG. 7. (Color online) Correlation functions for various structural indices: β (square), γ (triangle), Φ_{loc} (circle) and N (diamond).